

Activation-Based Sampling for Pixel- to Image-Level Aggregation in Weakly-Supervised Segmentation

Arvi Jonnarth* Michael Felsberg[†] Yushan Zhang
 Department of Electrical Engineering, Linköping University, Sweden
 {arvi.jonnarth, michael.felsberg, yushan.zhang}@liu.se

Abstract

Classification networks can be used to localize and segment objects in images by means of class activation maps (CAMs). However, without pixel-level annotations, they are known to (1) mainly focus on discriminative regions, and (2) to produce diffuse CAMs without well-defined prediction contours. In this work, we approach both problems with two contributions for improving CAM learning. First, we incorporate importance sampling based on the class-wise probability mass function induced by the CAMs to produce stochastic image-level class predictions. This results in CAMs which activate over a larger extent of the objects. Second, we formulate a feature similarity loss term which aims to match the prediction contours with edges in the image. As a third contribution, we conduct experiments on the PASCAL VOC and MS-COCO benchmark datasets to demonstrate that these modifications significantly increase the performance in terms of contour accuracy, while being comparable to current state-of-the-art methods in terms of region similarity.

1. Introduction

The great advancements of deep learning methods in recent years have had a large impact on many computer vision tasks, with no exception for semantic segmentation. The ability to automatically segment images has been found useful in many applications, including autonomous driving [1], video surveillance [2], and medical image analysis [3]. Fully-supervised segmentation frameworks have achieved remarkable results by utilizing large datasets of pixel-wise annotated images. However, these annotations require a significant manual labelling effort, which increases with the dataset size. Image-level weakly-supervised semantic segmentation (WSSS) aims to alleviate the labelling effort, where instead of requiring human-annotated pixel-wise seg-

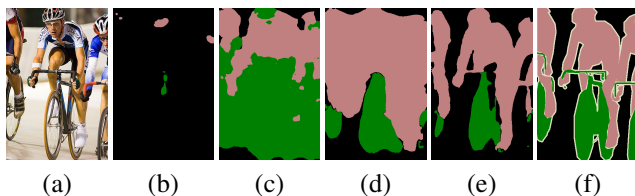


Figure 1. CAM comparison. (a) Input image; pseudo-labels with (b) max pooling, (c) SEAM [4] (average pooling) (d) importance sampling, and (e) importance sampling and feature similarity loss; (f) ground truth.

mentation masks, the only source of supervision are image-level classification labels. This opens the possibility to train segmentation models on existing large-scale datasets where pixel-level labels are non-existent and infeasible to acquire.

A common approach to WSSS is to first train a classification network with global average pooling (GAP) to produce class activation maps (CAMs) [5]. The CAMs are used to generate pseudo-labels for supervising the final segmentation network [4, 6, 7]. However, classification networks are known to (1) mainly focus on discriminative regions as opposed to the whole extent of objects, and (2) to produce overly smooth CAMs without well-defined prediction contours [5–7]. In this work, we improve the CAMs in these two aspects by substituting GAP with *importance sampling*. We sample from the class-wise probability mass function induced by the CAMs to produce stochastic image-level class predictions during training. This leads to CAMs which activate over a larger extent of objects, and not only on discriminative regions. Additionally, we formulate a new *feature similarity loss term*, which aims to match prediction contours with edges in the image. Our experiments show that this loss term significantly increases the contour quality. Figure 1 visualizes the benefits of our contributions. Finally, we perform experiments on the PASCAL VOC and MS-COCO benchmark datasets to demonstrate that our method is comparable to current state-of-the-art WSSS methods in terms of region similarity. A short early version of this work has been published at ICASSP [8].

*Affiliation: Husqvarna Group, Huskvarna, Sweden.

[†]Co-affiliation: University of KwaZulu-Natal, Durban, South Africa.

2. Related work

Weakly-supervised segmentation combines several different topics, for which we describe the related work below.

Types of weak supervision. Depending on the application and available data, one might have access to different types of annotations. Therefore, it is of interest to find methods which can learn to segment images based on various types of weak supervision. Semantic segmentation networks have successfully been trained in the past without access to full annotations in the form of segmentation masks. This has been achieved by utilizing different types of weak labels during training, such as bounding boxes [9–11], scribbles [12, 13], points [14] and classification labels, in decreasing levels of supervision. Classification labels have been the most popular as they require the least amount of manual labelling effort, and it is clear that they can be gathered from any of the stronger label types. Classification labels have been used for learning CAMs [4, 7] and pixel affinities [6], constraining the neural network output [15], seeding, expanding and constraining the segmentation predictions [16], as well as using them in combination with saliency maps [17], all in order to increase the quality of the segmentation predictions. In this work, we focus on the lowest level of weak supervision, that is, image-level classification labels.

Class activation maps. Class activation maps [5, 18] have been used to visualize what part of the input a neural network uses to base its prediction on. CAMs are usually produced using GAP in the final layers, where class predictions are propagated into pixel space. Due to their ability to give an indication of the position and size of objects without ground-truth segmentation masks, they have been adapted in many WSSS methods. Ahn et al. [6] use CAMs as a starting point for predicting pixel affinities, which they use to produce better segmentation predictions. Wang et al. [4] improve the generation of CAMs with a siamese network architecture and equivariant regularization to further improve results. Oquab et al. [19] use global max-pooling to produce image-level class predictions during training, where they use the activation maps for object localization. In this work, we choose a slightly different approach to previous methods by using random sampling instead of pooling to produce classification predictions. We show that this approach leads to better CAMs in terms of activating over the entire extent of objects as opposed to focusing on small discriminative regions. Therefore, it is well suited for the task of semantic segmentation. Lee et al. [7] also use stochasticity for improving CAMs, where they use spatial dropout for hidden unit selection in order to produce multiple localization maps during both training and inference. Our approach differs in two ways. First, we use a non-uniform sampling strategy based on the class activation maps for sampling image-level classification predictions. Second, we only use

it during training, thus employing a deterministic inference scheme.

Pixel- to image-level aggregation. Advanced pooling strategies have been extensively studied in the past, and some have suggested to use activation ranking which shares some similarities with importance sampling. Kolesnikov & Lampert [16] introduce global weighted rank-pooling (GWRP) which aggregates the pixel-level activations by ranking them and assigning a weight based on the rank. Durand et al. [20] combine the highest and lowest activations to form their spatial pooling strategy. Our approach differs in that neither of the previous works perform sampling, while they both include an implicit object size prior defined by method-related parameters.

Prediction-propagation based on feature similarities. The concept of propagating a signal to spatial neighbours based on feature similarities has been studied in the past, whether it be by computing a weighted mean of nearby pixels for image denoising [21], or by letting the raw image features define the pair-wise potentials in a fully connected conditional random field (CRF) for propagating initial segmentation predictions iteratively [22]. Ahn et al. introduce an additional network for learning class-agnostic pixel affinities [6]. More recently, prediction propagation has been used in an attention-based WSSS approach where the CAM predictions are propagated to similar pixels based on deep features in order to improve segmentation results [4]. In this work, we propose to do this implicitly through a class-specific *feature similarity loss term* based on pixel and prediction similarities, which is minimized when the prediction contours of CAMs match the edges in the image.

Model distillation. Many state-of-the-art WSSS methods [4, 7, 23] implicitly take advantage of model distillation, by applying the two-stage framework of first generating pseudo-labels using a classification network, and subsequently training a segmentation network on the generated pseudo-labels in a fully supervised setting. As has been demonstrated in the past [24, 25], large ensembles of models can be distilled into a single model without a significant loss of performance by training the final model to predict the output of the ensemble. Recently, it has also been shown that only one model is sufficient to be used as the “ensemble” to gain better results compared to simply training the final model directly on the data [26]. This is referred to as self-distillation. In a sense, the two-stage framework in WSSS is a form of self-distillation, and we also take advantage of this phenomenon by adapting the two stages in generating pseudo-labels for the final segmentation network.

3. Approach

In this section we describe our approach of training a network for predicting CAMs, and how we integrate our two main contributions for improving them.

3.1. Computing CAMs

Let $a_\theta(x) \in [0, 1]^{W \times H \times K}$ denote a class activation map (CAM) which is a function of the input image x , and parameterized by θ , where W , H and K denote the width, height and number of classes (including background) respectively. Furthermore, let $s_\theta(x)_{ijk}$ represent the unnormalized logit of class k at the position indexed by i and j . Typically, this is the output of the last convolutional layer without activation function. If we model the class probabilities in each pixel as a normalized probability distribution we can estimate the probability that a pixel contains a certain class k using the softmax function as

$$a_\theta(x)_{ijk} := \Pr(z_{ij} = k|x) = \frac{e^{s_\theta(x)_{ijk}}}{\sum_{t=1}^K e^{s_\theta(x)_{ijt}}}, \quad (1)$$

where $z \in \mathbb{R}^{W \times H}$ is the ground-truth segmentation mask and z_{ij} is the class index present at the pixel indexed by i and j . $\Pr(z_{ij} = k|x)$ is the estimated probability that class k is present in pixel (i, j) in a given image x .

Since z is unknown in the weakly supervised setting, the pixel-wise class predictions need to be condensed into an image-level prediction. Commonly, global average pooling (GAP) on the unnormalized logits has been used in WSSS for this purpose [4, 6]. In this case the image-level probability that class k is present in the image is given by the logistic function

$$\hat{y}_k^{GAP} = \frac{e^{s_k}}{e^{s_k} + 1}, \quad (2)$$

and where the image-wide average of the logits is given by

$$s_k = \frac{1}{HW} \sum_{ij} s_\theta(x)_{ijk}. \quad (3)$$

However, when minimizing a classification loss in this case, every pixel contributes to the loss. Thus, if an image contains an object of class k , the loss encourages the model to classify every pixel as belonging to that class. This might lead to over-activation, blurry class activations and poorly defined prediction contours, see for example the result of a GAP-based method in Fig. 1(c). Instead, we choose a different approach.

Assuming that, in order for an image to be classified as containing an object, it suffices that only one pixel contains that object, then we predict $\Pr(k \in \{z_{ij}\}_{i=1, j=1}^{W, H} | x)$. We sample a single pixel per class based on the probabilities a_θ since this essentially translates to “if at least one pixel contains an object, the whole image contains this object”. The first obvious option is to apply global max pooling for this purpose, where the predicted image-level probabilities can be written as

$$\hat{y}_k^{GMP} := \Pr\left(k \in \{z_{ij}\}_{i=1, j=1}^{W, H} | x\right) = \max_{ij} a_\theta(x)_{ijk}. \quad (4)$$

A shortcoming of max pooling is that it tends to activate over small discriminative regions and does not offer very useful segmentation predictions, even in cases where the classification prediction is correct. This can be observed in Fig. 1(b). To improve the CAMs in this regard we use *importance sampling* to produce stochastic image-level class predictions during training.

3.2. Importance sampling

As described in the previous section, global max pooling (GMP) tends to activate over small discriminative regions and does not leverage adequate segmentation predictions for pseudo-label generation. To solve this problem we introduce an additional image-level prediction by sampling one pixel for each class using the probability mass function induced by the class activation map a_θ . Let us define K probability mass functions, one for each class

$$p_k(I, J|x) = \Pr(I = i, J = j|x, k) = \frac{1}{Z_k(a)} a_\theta(x)_{ijk}, \quad (5)$$

where $Z_k(a) = \sum_{i=1}^W \sum_{j=1}^H a_\theta(x)_{ijk}$ is a normalizing constant. Now, we sample image coordinates for each class which we use to extract the class activations. These activations are then interpreted as classification predictions

$$\tilde{y}_k = a_\theta(x)_{\hat{i}\hat{j}k}, \quad (\hat{i}, \hat{j}) \sim p_k(I, J|x). \quad (6)$$

Had the distributions p_k been uniform, this method would be similar to GAP since each pixel would have been given the same weight. Note also that in this case the distributions would not be conditioned on the input image x . However, in the case of the activation-based distributions in Eq. (5), the probability mass depends on the class activations, and pixels with higher activations are more likely to be sampled. Furthermore, pixels with zero activation for a certain class are never sampled and do not contribute to the classification loss term for that class. Note also that since we use softmax in Eq. (1), at least one class will have a non-zero probability in every pixel.

We can further compare GAP and importance sampling by considering the case of small objects. With GAP, in order for a model to perform a correct image-level prediction that an object is present in the image, it would have to output large positive logits at the few pixels resembling the object while outputting small negative logits at the majority of pixels not part of the object. Therefore, the model is not encouraged to predict the absence of objects with high certainty, a constraint not present for importance sampling. Essentially, we avoid the problem of GAP, that pixels which are correctly classified as not containing an object get reflected negatively on the loss in cases where the object is present somewhere else in the image.

If the distributions had instead been defined as the Kronecker delta function and equal to 1 at the maximum acti-

vation, we would get max pooling. Similar to max pooling, we choose one pixel to represent the image-level prediction for each class, but we choose them randomly based on the class activations. This allows the model to activate over the whole extent of objects and not only on the most discriminative regions.

Due to the nature of convolutional neural networks, they tend not to activate only at a specific pixel, but rather over a region of pixels since the visual features are spatially correlated. Thus, for a model that under-activates, in the worst case we would sample pixels from a small region around discriminant features. Eventually, pixels at the prediction border would be sampled and the model would be encouraged to associate also these pixels with the object, thus covering a larger extent of it. Conversely, for a model that over-activates, pixels that do not correspond to object features would eventually be sampled. This behaviour is penalized in images where the feature is present but not the object. Thus, importance sampling encourages the model to activate only over the objects themselves.

The parameters θ can be found by minimizing the sum of K binary cross-entropy loss terms

$$\mathcal{L}_{ce}(y, \tilde{y}; \theta) = -\frac{1}{K} \sum_{k=1}^K y_k \log \tilde{y}_k + (1 - y_k) \log(1 - \tilde{y}_k), \quad (7)$$

where y_k is the image-level label for class k , which is equal to 1 if class k is present in the image and 0 otherwise. To understand how the behaviour shifts, we train our CAM network using a classification loss containing two cross-entropy terms, one for the prediction \hat{y} computed using either GMP or GAP, and one for the prediction \tilde{y} attained by random sampling according to Eq. (6). Our classification loss term is a convex combination of these two terms

$$\mathcal{L}_{cls}(y, \hat{y}, \tilde{y}) = (1 - \lambda) \mathcal{L}_{ce}(y, \hat{y}) + \lambda \mathcal{L}_{ce}(y, \tilde{y}), \quad (8)$$

where $\lambda \in [0, 1]$ is a parameter controlling the weight between the two cross-entropy terms. A value of $\lambda = 0$ corresponds to the case described in Sec. 3.1 with no importance sampling, and a value of $\lambda = 1$ corresponds to only using stochastic predictions during training. While the first cross-entropy term has been successful in classification tasks, it is unclear whether the first, second or a combination of the two is most suitable for weakly-supervised segmentation.

In our early experiments we observed that importance sampling improved the CAMs in terms of covering a larger extent of the objects, but the prediction borders did not align with their edges, see Fig. 1(d). For this reason we introduce a *feature similarity loss term*, which aims to match the prediction contours with the edges of objects.

3.3. Feature similarity loss

Intuitively, similar pixels that are in close proximity have a high probability of being part of the same object. Additionally, if two nearby pixels are dissimilar, there is a chance that they belong to different classes and that the contour runs somewhere between them. Based on this rationale, we formulate a loss term which penalizes dissimilar predictions for nearby similar pixels. Furthermore, similar predictions are discouraged for nearby dissimilar pixels if their predictions are sufficiently dissimilar to begin with. We also find it beneficial to learn the cross-over point of what should be considered as sufficiently dissimilar. In what follows, we formulate our feature similarity loss term as a function of the pixel-wise class predictions and features. Subsequently, we describe the intuition behind our formulation.

In the following equations we use a single index for the image coordinates in order to reduce notational clutter. Let us define a gating function $g(a_i, a_j) : \mathbb{R}^{2K} \rightarrow \mathbb{R}_+$ which computes the distance between the predictions a_i and a_j of the pixels i and j , as well as a function $f(\delta) : [0, 1] \rightarrow [-1, 1]$ which maps the dissimilarity $\delta(x_i, x_j) \in [0, 1]$ between the features x_i and x_j monotonically to $[-1, 1]$. Furthermore, we formulate the feature similarity loss term

$$\mathcal{L}_{fs}(a, x) = -\frac{1}{(HW)^2} \sum_{ij} w_{ij} g(a_i, a_j) f(\delta(x_i, x_j)), \quad (9)$$

where the weight w_{ij} is a function of the distance between pixels i and j and is used to give a higher weight to pixel pairs which are close to each other. Note that a_i and x_i are vectors representing respectively the class probability distribution and image features for pixel i . Throughout our experiments we define the weights using a Gaussian neighbourhood

$$w_{ij} = \frac{1}{2\pi\sigma^2} \exp\left(-\frac{\|p_i - p_j\|_2^2}{2\sigma^2}\right), \quad (10)$$

where p_i and p_j are two-dimensional vectors containing the image coordinates of pixels i and j , and σ is the standard deviation of the Gaussian function to control the size of the considered pixel neighbourhood. Furthermore, we define the gating function g as the squared L^2 distance between the predictions

$$g(a_i, a_j) = \frac{1}{2} \|a_i - a_j\|_2^2, \quad (11)$$

and the function f as

$$f(\delta(x_i, x_j)) = \tanh\left(\mu + \log\left(\frac{\delta}{1 - \delta}\right)\right), \quad (12)$$

where μ is a bias parameter. The logarithm in Eq. (12) computes the logit of the binary decision problem whether or not

two pixels are (dis)similar. The tanh function then maps the logit with the added bias from \mathbb{R} onto the interval $[-1, 1]$. Thus, f takes the values -1 and $+1$ when pixels are similar ($\delta = 0$) and dissimilar ($\delta = 1$) respectively, and μ controls the cross-over point at which f changes sign.

For two similar pixels, we have $f < 0$ and get $\mathcal{L}_{fs} \geq 0$ since $g \geq 0$. \mathcal{L}_{fs} is thus minimized if g is minimized, i.e. if $a_i = a_j$. In the case of two dissimilar pixels on the other hand, i.e. if $f > 0$, we have $\mathcal{L}_{fs} \leq 0$, which is minimized if g is maximized, which occurs when a_i and a_j are opposite predictions, i.e. if they are two one-hot vectors predicting different classes. However, it is not always the case that two dissimilar pixels are part of different classes. For example, an object could contain some high-frequency texture or be made up of several parts with different visual appearance. However, since the gating function is chosen to be the squared L^2 distance, the gradient of \mathcal{L}_{fs} with respect to the predictions is proportional to the difference between the predictions, and equal to zero if $a_i = a_j$. Consequently, if two pixels have similar predictions, only a small gradient is propagated through the feature similarity loss, and the total gradient is dominated by the classification loss. This allows the network to classify larger regions to the same class, even though they contain parts with dissimilar features. Thus, the network can activate over the whole extent of objects.

Instead of manually finding good values for the standard deviation σ in Eq. (10) and the bias parameter μ in Eq. (12), we learn them together with the network parameters θ during training. Furthermore, we use RGB pixel values in $[0, 1]$ for the features x , and choose the dissimilarity $\delta = \|x_i - x_j\|_1 / C$, which has been used in stereo matching [27], where $C = 3$ is the dimensionality of the feature vectors. Although learnable features would allow for finding image-specific biases, they could potentially lead to trivial solutions or unwanted behaviours if combined with the classification loss, as we would essentially be learning the loss function. Therefore, we stick to RGB features.

4. Experiments

This section outlines the experimental results achieved for the methods described above, including implementation details, extensive ablation studies, baseline comparisons, and a comparison with state-of-the-art WSSS methods.

4.1. Implementation details

Datasets. For training and evaluation we use the *PASCAL Visual Object Classes* (VOC) dataset [28] containing 1,464 training images, 1,449 validation images and 1,456 hold-out test images, with 20 foreground classes. Furthermore, we include the training data proposed by Hariharan et al. [29], which is common in VOC experiments, resulting in a total of 10,582 training images. We also perform experiments on the larger *MS Common Objects in*

Context (COCO) dataset [30] containing 82,783/118,287 training images and 40,504/5,000 validation images for the 2014/2017 train-val splits, with 80 foreground classes. Although ground-truth segmentation masks are available, we only use image-level classification labels for training.

Training details. For our CAM network we use the same siamese architecture as our baseline method SEAM [4] with a ResNet-38 [31] backbone. As part of the architecture, we also incorporate their method of refining the CAMs using a pixel correlation module (PCM) in the final layer of the network, and adopt their equivariant regularization (ER) and equivariant cross regularization (ECR) loss terms. Thus, our loss function has four terms, namely \mathcal{L}_{cls} , \mathcal{L}_{fs} , \mathcal{L}_{er} and \mathcal{L}_{ecr} . We simply sum the four terms, corresponding to a weight of 1 for each of the terms, which has also been done in SEAM (for \mathcal{L}_{cls} , \mathcal{L}_{er} , and \mathcal{L}_{ecr}). We perform minor adjustments to the forward method of the network and the inference scheme to fit with our probabilistic formulation according to Eqs. (1), (5) and (6). In order to measure the effects of our contributions we do not change any settings or hyperparameters, such as input image dimensions, data augmentation, batch size, number of epochs, optimizer, learning rate, or learning rate schedule. For a fair comparison, we follow the framework in SEAM of training an AffinityNet [6] to further refine the CAMs before pseudo-label generation. During AffinityNet label generation, we modify the background parameter α to 2 and 4 when amplifying and weakening the background activations respectively. This was necessary as the values in our CAMs were distributed close to either 0 or 1, while the CAMs from SEAM were distributed more evenly over $[0, 1]$. Other than that, we use the same settings and hyperparameters. As the last step, we train a DeepLab-v1 [32] network as our final segmentation model which is supervised by our generated pseudo-labels from the CAM and AffinityNet networks. Both the AffinityNet and DeepLab-v1 networks have the same ResNet-38 [31] backbone as our CAM network. Similar to SEAM, we use CRF [22] to produce our segmentation predictions during inference. In our experiments we use two A100 40GB GPUs.

Evaluation metrics. For evaluation, we use the commonly adopted mean intersection-over-union (mIoU) metric based on the area of the segmentations to measure region similarity. Furthermore, we use the F-score computed on the contours, which has previously been used to measure contour accuracy in video object segmentation [33]. Our choice of using both area and contour metrics is motivated by the fact that they evaluate complementary aspects. Depending on the downstream task, one aspect might be more important than the other. For example, contours contribute more to the perceived visual quality [34], and bears more weight in cases where the segmentations are displayed to a human, such as in virtual green-screen applications. Since

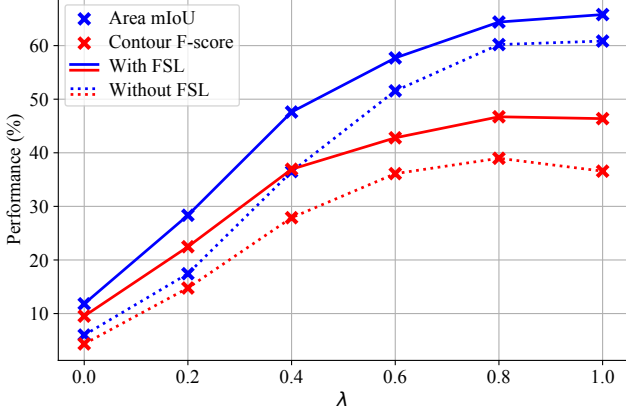


Figure 2. Performance as a function of the loss parameter λ and the feature similarity loss (FSL) when using global max pooling on the VOC validation set.

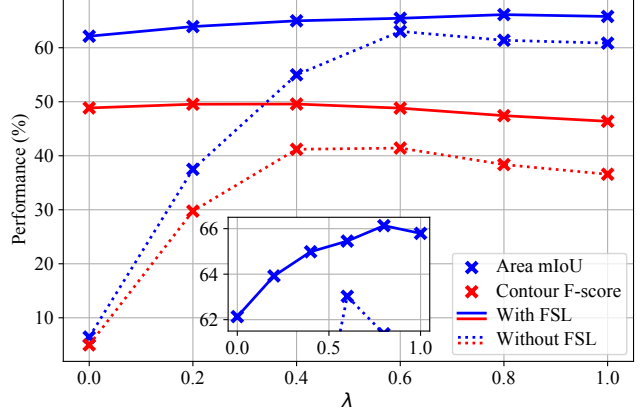


Figure 3. Performance as a function of the loss parameter λ and the feature similarity loss (FSL) when using global average pooling on the VOC validation set.

we do not consider a specific application, it is important to evaluate both aspects simultaneously. We adapt the code¹ from Perazzi et al. [33] and compute the F-score by first accumulating bipartite matches of the boundaries between the predicted and ground-truth masks, efficiently approximated using morphological operations. Subsequently, we compute the class-wise F-scores over the dataset, which we then average. Although the VOC segmentation masks contain a thin no-class region between objects, the contour F-score still gives a clear indication of the contour quality since we match the boundaries using dilated regions. Thus, we compute the contour accuracy by considering this no-class region as background.

4.2. Ablation study

To investigate the effects of the *importance sampling* and *feature similarity loss* (FSL) we train our CAM network on the VOC dataset and compare region similarity in terms of mIoU based on the area of predicted segmentations, as well as contour accuracy in terms of the F-score computed on the contours. We compute these metrics on the validation set for the predictions of our trained DeepLab-v1 model.

In Figs. 2 and 3 we sweep the loss parameter λ from Eq. (8) for global max pooling (GMP) and global average pooling (GAP) respectively, and plot the area mIoU and contour F-score. With max pooling in Fig. 2 we observe a significant increase in segmentation performance when increasing λ , both in terms of region similarity and contour accuracy. The highest performance in terms of region similarity occurs at $\lambda = 1$, and for contour accuracy at around 0.8. This is due to the fact that the classification loss is computed based on more than just the most activated pixel and thus encourages the model to activate not only over the most discriminant feature. If the model activates

over any feature that distinguishes a certain class, those pixels will be sampled during training and thus the model can learn to associate these features to the corresponding class. We can observe this in Fig. 1. With GMP only, the model activates over the most discriminant features, e.g. the faces of the persons. With importance sampling, it has learned to activate also over other features, such as hands and legs. Similarly, if the model activates over features that are not associated with a certain class it will get penalized in cases where those features are present but not the class. Thus, it will learn to activate only over the objects themselves.

With GAP in Fig. 3 we see a similar trend of better region similarity for larger values of λ . However, the maximum occurs at $\lambda = 0.8$ which indicates that a combination of GAP and importance sampling is better than using only one or the other. We hypothesize that average pooling contributes with a regularizing effect by effectively introducing a bias to the probability distributions p_k in Eq. (5). As explained in Sec. 3.2, GAP corresponds to a uniform distribution. The combination of GAP and importance sampling would then correspond to using a mixture of the activation-based and uniform distributions, and the resulting distribution would be similar to the activation-based distribution but with a non-zero minimum, i.e. a bias. The specific value of $\lambda = 0.8$ indicates that this bias should be quite small. The maximum for the contour F-score occurs at a different value of λ , at around 0.4. However, since the main evaluation metric for WSSS is area mIoU, we choose $\lambda = 0.8$ with GAP for the rest of our experiments, unless stated otherwise. Furthermore, with FSL, we observe a performance boost for both GMP and GAP for all values of λ . Therefore, we include it in the rest of our experiments.

A reasonable hypothesis is that sampling several pixels could allow for more efficient learning and better CAMs. However, we observed that the number of sampled pixels had no significant effect, see Appendix B. Therefore, we

¹Code adapted from (BSD 3-Clause License): <https://github.com/davisvideochallenge/davis2017-evaluation/>

Table 1. Performance on the COCO 2014/2017 *val* sets with GAP.

λ	Area mIoU		Contour F-score	
	2014	2017	2014	2017
0.8	28.8	32.7	25.7	27.9
0.9	32.2	33.3	28.2	27.8
1	30.0	30.6	26.4	26.8

Table 2. Baseline comparison with SEAM [4] on the VOC *validation* set. Contour F-scores for SEAM were computed by us.

	Area mIoU		Contour F-score	
	SEAM	Ours	SEAM	Ours
CAMs	52.5	55.0	20.8	39.7
+ AffinityNet	60.1	63.9	35.7	48.6
+ DeepLab-v1	64.5	66.1	38.2	47.4

sample only one pixel per class since it requires the least amount of computations.

We perform further experiments on the more challenging MS-COCO dataset. Table 1 shows the performance of the final segmentation predictions for three different values of λ using GAP. We see a similar behaviour compared to VOC, except that the maximum area mIoU occurs at $\lambda = 0.9$. This is reasonable in the sense that the large amount of training data reduces the need for regularization, and thus a higher value for λ is more suitable.

For a qualitative assessment, we display in Fig. 4 the foreground class activations, together with CAM pseudo-labels and final predictions on the VOC dataset. Our method manages to successfully segment the images with impressive contour quality, even in low contrast conditions, e.g. black suit on dark background, while being less successful on thin structures, e.g. boat masts and table/chair legs.

4.3. Baseline comparison

We use the code provided by Wang et al. [4] to train an AffinityNet² and DeepLab-v1³ model, but with SEAM as the CAM network. To compare our results, we compute the area mIoU and contour F-score in the three stages of training for both methods. Table 2 shows the results on the VOC validation set. Note that the first two rows comparing CAM and AffinityNet results show the metrics computed for pseudo-labels without CRF. The last row compares the results between the final segmentation predictions where CRF has been applied. We observe that our method has significantly better contour accuracy across the board, where the difference is most notable for the CAM results. Furthermore, the property of accurate contours carries through to

²Code (MIT License): <https://github.com/YudeWang/SEAM>

³Code (MIT License): <https://github.com/YudeWang/semantic-segmentation-codebase>

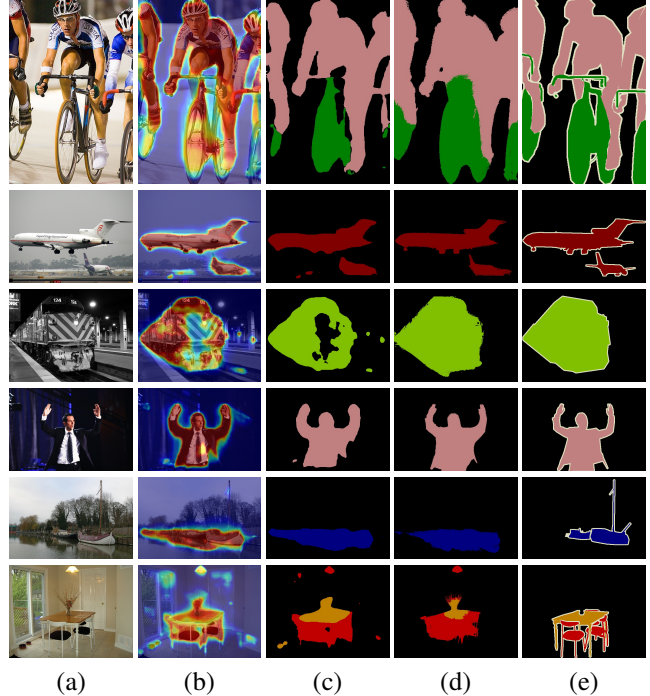


Figure 4. Qualitative segmentation results. (a) Input image, (b) foreground class activations, (c) pseudo-labels from our CAM network, (d) final segmentation predictions and (e) ground-truth segmentations. The bottom two rows illustrate failure cases.

the final segmentation model. Both methods benefit from training an AffinityNet where the contour accuracy and region similarity increase for both methods. We also observe an improvement in terms of region similarity where we reach 66.1 mIoU compared to 64.5 for SEAM.

4.4. State-of-the-art comparison

We compare our results with state-of-the-art WSSS methods on the VOC dataset in Tab. 3, where our method reaches similar performance in terms of region similarity. We also include results on the COCO dataset for the subset of methods for which this has been reported. Some methods make use of additional supervision, either directly using more data, or indirectly using saliency maps. These have been excluded from the comparison, but can be found in Appendix A. A few methods also perform experiments on more powerful backbones, such as Res2Net-101 [35]. For a more backbone-agnostic and fair comparison we only include results for the most common backbones VGG-16 [36], ResNet-38 [31], and ResNet-101 [37].

In Tab. 4 we compare contour F-score with our baseline SEAM [4] and the best region similarity method PMM [38], where the contour quality of our method is superior. Furthermore, if we do as in the well-established DAVIS benchmark for video object segmentation [33] and consider the the two metrics equally, we outright outperform both meth-

Table 3. Area mIoU on the VOC 2012 val/test sets, and COCO 2014/2017 val sets (trained on their respective training sets).

Method	VOC		COCO	
	<i>val</i>	<i>test</i>	2014	2017
CCNN [15]	35.3	35.6	-	-
EM-Adapt [11]	38.2	39.6	-	-
SEC [16]	50.7	51.7	-	-
AugFeed [39]	54.3	55.5	-	-
AffinityNet [6]	61.7	63.7	-	-
ICD [40]	64.1	64.3	-	-
CIAN [41]	64.3	65.3	-	-
SSDD [42]	64.9	65.5	-	-
SEAM [4]	64.5	65.7	-	-
CONTA [43]	66.1	66.7	33.4	-
CDA [44]	66.1	66.8	33.7	-
MCIS [45]	66.2	66.9	-	-
ECS-Net [46]	66.6	67.6	-	-
CGNet [47]	68.4	68.2	36.4	-
CPN [48]	67.8	68.5	-	-
PMM [38]	68.5	69.0	36.7	-
Ours	66.1	66.6	32.2	33.3

Table 4. Contour F-score on the VOC *val* set for pseudo-labels.

Method	Backbone	F-score
SEAM [4]	ResNet-38 [31]	35.7
PMM [38]	ResNet-38 [31]	42.1
PMM [38]	ScaleNet-101 [49]	42.4
Ours	ResNet-38 [31]	48.6

ods. Thus, in applications where contour quality bears even a small importance, our method is preferable.

5. Discussion

Limitations and future research. In the previous section we highlighted the advantages of our method, but some limitations exist, which we discuss here. A general limitation for weakly supervised methods is their performance compared to their fully supervised counterparts. This deficit is of course traded for a much cheaper labelling cost, but it is important to keep in mind in case an application requires very high segmentation performance. Another limitation for weakly-supervised models is that they have a hard time segmenting thin structures, such as boat masts or chair and table legs, which can be seen in Fig. 4. To this end, it would be interesting to investigate how shape priors [50] could be utilized. Although we have shown that our contributions can be implemented for a GAP-based approach, it is not clear that they generalize to other state-of-the-art baselines. It would therefore be interesting to implement

our contributions on other existing methods. Furthermore, we have only performed experiments on two datasets of natural images. It would be interesting to evaluate our method on different image domains, such as satellite or medical images. On the COCO dataset, we observed limited performance on tail classes, e.g. toaster and hair dryer. The reason for this could be investigated in future research to find a solution, and to potentially increase performance further. As a final remark, we have combined global pooling methods with importance sampling by using a convex combination of two loss terms. However, as discussed in the paper, max and average pooling correspond to specific sampling distributions. Therefore, it would be interesting to modify the distributions directly, e.g. by raising them to a power, in order to interpolate between the different approaches.

Societal impacts. Image segmentation has several applications, including autonomous driving [1], medical image analysis [3], and video surveillance [2]. Although we have not focused on any specific application in this work, we describe some potential societal impacts in regard to image segmentation in general. Autonomous vehicles lead to lower greenhouse gas emissions, improved traffic safety, and frees up time for people [51]. Automated medical image analysis can be used to aid doctors in identifying sick patients [52], and video surveillance can be used for crime prevention [53]. Video surveillance could have potential negative impacts as well, such as being used for compromising integrity, mass surveillance, and data harvesting. However, the models considered in this work are trained in the weakly-supervised setting and lack the ability to discriminate based on specific human traits. For deep learning in general, the training of huge models could have negative environmental impacts, and it is important to assess the task at hand whether they are outweighed by the potential positive impacts that the models can provide.

Conclusions. In this paper, we present two methods for improving segmentation predictions in weakly-supervised semantic segmentation. First, we use importance sampling for producing image-level classification predictions during training, which results in CAMs that activate over a larger extent of the objects. Second, we propose a new loss term for matching prediction contours with edges in the image. We show experimentally that this significantly improves the contour quality of our segmentation predictions. Finally, we perform experiments on the PASCAL VOC and MS-COCO benchmark datasets to show that our method is comparable to state-of-the-art methods in terms of region similarity.

6. Acknowledgements

This work was partially supported by the Wallenberg AI, Autonomous Systems and Software Program (WASP) funded by the KAW foundation, and SNIC, partially funded by VR through grant agreement no. 2018-05973.

References

- [1] Marius Cordts, Mohamed Omran, Sebastian Ramos, Timo Rehfeld, Markus Enzweiler, Rodrigo Benenson, Uwe Franke, Stefan Roth, and Bernt Schiele. The cityscapes dataset for semantic urban scene understanding. In *Proceedings of the IEEE Conference on Computer Vision and Pattern Recognition (CVPR)*, 2016. 1, 8
- [2] Monica Gruosso, Nicola Capece, and Ugo Erra. Human segmentation in surveillance video with deep learning. *Multimedia Tools and Applications*, 80(1):1175–1199, 2021. 1, 8
- [3] Shervin Minaee, Yuri Y. Boykov, Fatih Porikli, Antonio J Plaza, Nasser Kehtarnavaz, and Demetri Terzopoulos. Image segmentation using deep learning: A survey. *IEEE Transactions on Pattern Analysis and Machine Intelligence*, 2021. 1, 8
- [4] Yude Wang, Jie Zhang, Meina Kan, Shiguang Shan, and Xilin Chen. Self-supervised equivariant attention mechanism for weakly supervised semantic segmentation. In *Proceedings of the IEEE/CVF Conference on Computer Vision and Pattern Recognition*, pages 12275–12284, 2020. 1, 2, 3, 5, 7, 8, 12, 13
- [5] Bolei Zhou, Aditya Khosla, Agata Lapedriza, Aude Oliva, and Antonio Torralba. Learning deep features for discriminative localization. In *Proceedings of the IEEE Conference on Computer Vision and Pattern Recognition*, pages 2921–2929, 2016. 1, 2
- [6] Jiwoon Ahn and Suha Kwak. Learning pixel-level semantic affinity with image-level supervision for weakly supervised semantic segmentation. In *Proceedings of the IEEE Conference on Computer Vision and Pattern Recognition*, pages 4981–4990, 2018. 1, 2, 3, 5, 8, 13
- [7] Jungbeom Lee, Eunji Kim, Sungmin Lee, Jangho Lee, and Sungroh Yoon. Ficklenet: Weakly and semi-supervised semantic image segmentation using stochastic inference. In *Proceedings of the IEEE/CVF Conference on Computer Vision and Pattern Recognition*, pages 5267–5276, 2019. 1, 2, 13
- [8] Arvi Jonnarth and Michael Felsberg. Importance sampling CAMs for weakly-supervised segmentation. In *IEEE International Conference on Acoustics, Speech, and Signal Processing (ICASSP)*, 2022. 1
- [9] Jifeng Dai, Kaiming He, and Jian Sun. Boxesup: Exploiting bounding boxes to supervise convolutional networks for semantic segmentation. In *Proceedings of the IEEE International Conference on Computer Vision*, pages 1635–1643, 2015. 2
- [10] Anna Khoreva, Rodrigo Benenson, Jan Hosang, Matthias Hein, and Bernt Schiele. Simple does it: Weakly supervised instance and semantic segmentation. In *Proceedings of the IEEE Conference on Computer Vision and Pattern Recognition*, pages 876–885, 2017. 2
- [11] George Papandreou, Liang-Chieh Chen, Kevin P Murphy, and Alan L Yuille. Weakly- and semi-supervised learning of a deep convolutional network for semantic image segmentation. In *Proceedings of the IEEE International Conference on Computer Vision*, pages 1742–1750, 2015. 2, 8, 13
- [12] Di Lin, Jifeng Dai, Jiaya Jia, Kaiming He, and Jian Sun. Scribblesup: Scribble-supervised convolutional networks for semantic segmentation. In *Proceedings of the IEEE Conference on Computer Vision and Pattern Recognition*, pages 3159–3167, 2016. 2
- [13] Paul Vernaza and Manmohan Chandraker. Learning random-walk label propagation for weakly-supervised semantic segmentation. In *Proceedings of the IEEE Conference on Computer Vision and Pattern Recognition*, pages 7158–7166, 2017. 2
- [14] Amy Bearman, Olga Russakovsky, Vittorio Ferrari, and Li Fei-Fei. What’s the point: Semantic segmentation with point supervision. In *European Conference on Computer Vision*, pages 549–565. Springer, 2016. 2
- [15] Deepak Pathak, Philipp Krähenbühl, and Trevor Darrell. Constrained convolutional neural networks for weakly supervised segmentation. In *Proceedings of the IEEE International Conference on Computer Vision*, pages 1796–1804, 2015. 2, 8, 13
- [16] Alexander Kolesnikov and Christoph H Lampert. Seed, expand and constrain: Three principles for weakly-supervised image segmentation. In *European Conference on Computer Vision*, pages 695–711. Springer, 2016. 2, 8, 13
- [17] Yunchao Wei, Xiaodan Liang, Yunpeng Chen, Xiaohui Shen, Ming-Ming Cheng, Jiashi Feng, Yao Zhao, and Shuicheng Yan. Stc: A simple to complex framework for weakly-supervised semantic segmentation. *IEEE Transactions on Pattern Analysis and Machine Intelligence*, 39(11):2314–2320, 2016. 2, 13
- [18] Ramprasaath R Selvaraju, Michael Cogswell, Abhishek Das, Ramakrishna Vedantam, Devi Parikh, and Dhruv Batra. Grad-cam: Visual explanations from deep networks via gradient-based localization. In *Proceedings of the IEEE International Conference on Computer Vision*, pages 618–626, 2017. 2
- [19] Maxime Oquab, Léon Bottou, Ivan Laptev, and Josef Sivic. Is object localization for free? - weakly-supervised learning with convolutional neural networks. In *Proceedings of the IEEE Conference on Computer Vision and Pattern Recognition*, pages 685–694, 2015. 2
- [20] Thibaut Durand, Taylor Mordan, Nicolas Thome, and Matthieu Cord. WILDCAT: Weakly supervised learning of deep convnets for image classification, pointwise localization and segmentation. In *Proceedings of the IEEE Conference on Computer Vision and Pattern Recognition*, pages 642–651, 2017. 2
- [21] Antoni Buades, Bartomeu Coll, and Jean-Michel Morel. Non-local means denoising. *Image Processing On Line*, 1:208–212, 2011. 2
- [22] Philipp Krähenbühl and Vladlen Koltun. Efficient inference in fully connected crfs with gaussian edge potentials. *Advances in Neural Information Processing Systems*, 24:109–117, 2011. 2, 5

- [23] Yun Liu, Yu-Huan Wu, Pei-Song Wen, Yu-Jun Shi, Yu Qiu, and Ming-Ming Cheng. Leveraging instance-, image- and dataset-level information for weakly supervised instance segmentation. *IEEE Transactions on Pattern Analysis and Machine Intelligence*, 2020. 2, 13
- [24] Cristian Buciluă, Rich Caruana, and Alexandru Niculescu-Mizil. Model compression. In *Proceedings of the 12th ACM SIGKDD International Conference on Knowledge Discovery and Data Mining*, pages 535–541, 2006. 2
- [25] Geoffrey Hinton, Oriol Vinyals, and Jeff Dean. Distilling the knowledge in a neural network. *arXiv preprint arXiv:1503.02531*, 2015. 2
- [26] Zeyuan Allen-Zhu and Yuanzhi Li. Towards understanding ensemble, knowledge distillation and self-distillation in deep learning. *arXiv preprint arXiv:2012.09816*, 2020. 2
- [27] Mikel Galar, Aranzazu Jurio, Carlos Lopez-Molina, Daniel Paternain, Jose Sanz, and Humberto Bustince. Aggregation functions to combine rgb color channels in stereo matching. *Optics express*, 21(1):1247–1257, 2013. 5
- [28] Mark Everingham, Luc Van Gool, Christopher KI Williams, John Winn, and Andrew Zisserman. The pascal visual object classes (voc) challenge. *International Journal of Computer Vision*, 88(2):303–338, 2010. 5
- [29] Bharath Hariharan, Pablo Arbeláez, Lubomir Bourdev, Subhransu Maji, and Jitendra Malik. Semantic contours from inverse detectors. In *2011 International Conference on Computer Vision*, pages 991–998. IEEE, 2011. 5
- [30] Tsung-Yi Lin, Michael Maire, Serge Belongie, James Hays, Pietro Perona, Deva Ramanan, Piotr Dollár, and C Lawrence Zitnick. Microsoft coco: Common objects in context. In *European Conference on Computer Vision*, pages 740–755. Springer, 2014. 5
- [31] Zifeng Wu, Chunhua Shen, and Anton Van Den Hengel. Wider or deeper: Revisiting the resnet model for visual recognition. *Pattern Recognition*, 90:119–133, 2019. 5, 7, 8
- [32] Liang-Chieh Chen, George Papandreou, Iasonas Kokkinos, Kevin Murphy, and Alan L Yuille. Semantic image segmentation with deep convolutional nets and fully connected crfs. In *International Conference on Learning Representations*, 2015. 5
- [33] Federico Perazzi, Jordi Pont-Tuset, Brian McWilliams, Luc Van Gool, Markus Gross, and Alexander Sorkine-Hornung. A benchmark dataset and evaluation methodology for video object segmentation. In *Proceedings of the IEEE Conference on Computer Vision and Pattern Recognition*, pages 724–732, 2016. 5, 6, 7
- [34] Gabriela Csurka, Diane Larlus, and Florent Perronnin. What is a good evaluation measure for semantic segmentation? In *Proceedings of the British Machine Vision Conference (BMVC)*, volume 27, 2013. 5
- [35] Shang-Hua Gao, Ming-Ming Cheng, Kai Zhao, Xin-Yu Zhang, Ming-Hsuan Yang, and Philip Torr. Res2net: A new multi-scale backbone architecture. *IEEE Transactions on Pattern Analysis and Machine Intelligence*, 43(2):652–662, 2021. 7
- [36] Karen Simonyan and Andrew Zisserman. Very deep convolutional networks for large-scale image recognition. In *International Conference on Learning Representations*, 2015. 7
- [37] Kaiming He, Xiangyu Zhang, Shaoqing Ren, and Jian Sun. Deep residual learning for image recognition. In *Proceedings of the IEEE Conference on Computer Vision and Pattern Recognition*, pages 770–778, 2016. 7
- [38] Yi Li, Zhanghui Kuang, Liyang Liu, Yimin Chen, and Wayne Zhang. Pseudo-mask matters in weakly-supervised semantic segmentation. In *Proceedings of the IEEE/CVF International Conference on Computer Vision (ICCV)*, pages 6964–6973, October 2021. 7, 8, 13
- [39] Xiaojuan Qi, Zhengzhe Liu, Jianping Shi, Hengshuang Zhao, and Jiaya Jia. Augmented feedback in semantic segmentation under image level supervision. In *European Conference on Computer Vision*, pages 90–105. Springer, 2016. 8, 13
- [40] Junsong Fan, Zhaoxiang Zhang, Chunfeng Song, and Tieniu Tan. Learning integral objects with intra-class discriminator for weakly-supervised semantic segmentation. In *Proceedings of the IEEE/CVF Conference on Computer Vision and Pattern Recognition*, pages 4283–4292, 2020. 8, 13
- [41] Junsong Fan, Zhaoxiang Zhang, Tieniu Tan, Chunfeng Song, and Jun Xiao. Cian: Cross-image affinity net for weakly supervised semantic segmentation. In *Proceedings of the AAAI Conference on Artificial Intelligence*, volume 34, pages 10762–10769, 2020. 8, 13
- [42] Wataru Shimoda and Keiji Yanai. Self-supervised difference detection for weakly-supervised semantic segmentation. In *Proceedings of the IEEE/CVF International Conference on Computer Vision*, pages 5208–5217, 2019. 8, 13
- [43] Dong Zhang, Hanwang Zhang, Jinhui Tang, Xian-Sheng Hua, and Qianru Sun. Causal intervention for weakly-supervised semantic segmentation. In H. Larochelle, M. Ranzato, R. Hadsell, M. F. Balcan, and H. Lin, editors, *Advances in Neural Information Processing Systems*, volume 33, pages 655–666. Curran Associates, Inc., 2020. 8, 13
- [44] Yukun Su, Ruizhou Sun, Guosheng Lin, and Qingyao Wu. Context decoupling augmentation for weakly supervised semantic segmentation. In *Proceedings of the IEEE/CVF International Conference on Computer Vision (ICCV)*, pages 7004–7014, October 2021. 8, 13
- [45] Guolei Sun, Wenguan Wang, Jifeng Dai, and Luc Van Gool. Mining cross-image semantics for weakly supervised semantic segmentation. In *European conference on computer vision*, pages 347–365. Springer, 2020. 8, 13
- [46] Kunyang Sun, Haoqing Shi, Zhengming Zhang, and Yongming Huang. Ecs-net: Improving weakly supervised semantic segmentation by using connections between class activation maps. In *Proceedings of the IEEE/CVF International Conference on Computer Vision (ICCV)*, pages 7283–7292, October 2021. 8, 13

- [47] Hyeokjun Kweon, Sung-Hoon Yoon, Hyeonseong Kim, Daehee Park, and Kuk-Jin Yoon. Unlocking the potential of ordinary classifier: Class-specific adversarial erasing framework for weakly supervised semantic segmentation. In *Proceedings of the IEEE/CVF International Conference on Computer Vision (ICCV)*, pages 6994–7003, October 2021. 8, 13
- [48] Fei Zhang, Chaochen Gu, Chenyue Zhang, and Yuchao Dai. Complementary patch for weakly supervised semantic segmentation. In *Proceedings of the IEEE/CVF International Conference on Computer Vision*, pages 7242–7251, 2021. 8, 13
- [49] Yi Li, Zhanghui Kuang, Yimin Chen, and Wayne Zhang. Data-driven neuron allocation for scale aggregation networks. In *Proceedings of the IEEE/CVF Conference on Computer Vision and Pattern Recognition*, pages 11526–11534, 2019. 8
- [50] Daniel Cremers. Nonlinear dynamical shape priors for level set segmentation. In *IEEE Conference on Computer Vision and Pattern Recognition (CVPR)*, 2007. 8
- [51] Walter Brenner and Andreas Herrmann. *An Overview of Technology, Benefits and Impact of Automated and Autonomous Driving on the Automotive Industry*, pages 427–442. Springer Berlin Heidelberg, Berlin, Heidelberg, 2018. 8
- [52] Neeraj Sharma and Lalit M Aggarwal. Automated medical image segmentation techniques. *Journal of Medical Physics*, 35(1):3, 2010. 8
- [53] Eric L Piza, Brandon C Welsh, David P Farrington, and Amanda L Thomas. Cctv surveillance for crime prevention: A 40-year systematic review with meta-analysis. *Criminology & Public Policy*, 18(1):135–159, 2019. 8
- [54] Yunchao Wei, Jiashi Feng, Xiaodan Liang, Ming-Ming Cheng, Yao Zhao, and Shuicheng Yan. Object region mining with adversarial erasing: A simple classification to semantic segmentation approach. In *Proceedings of the IEEE conference on computer vision and pattern recognition*, pages 1568–1576, 2017. 13
- [55] Yunchao Wei, Huaxin Xiao, Honghui Shi, Zequn Jie, Jiashi Feng, and Thomas S Huang. Revisiting dilated convolution: A simple approach for weakly- and semi-supervised semantic segmentation. In *Proceedings of the IEEE Conference on Computer Vision and Pattern Recognition*, pages 7268–7277, 2018. 13
- [56] Xiang Wang, Shaodi You, Xi Li, and Huimin Ma. Weakly-supervised semantic segmentation by iteratively mining common object features. In *Proceedings of the IEEE Conference on Computer Vision and Pattern Recognition*, pages 1354–1362, 2018. 13
- [57] Puneet Kumar Dokania Arslan Chaudhry and Philip Torr. Discovering class-specific pixels for weakly-supervised semantic segmentation. In *Proceedings of the British Machine Vision Conference (BMVC)*, pages 20.1–20.13. BMVA Press, September 2017. 13
- [58] Qibin Hou, PengTao Jiang, Yunchao Wei, and Ming-Ming Cheng. Self-erasing network for integral object attention. In *Advances in Neural Information Processing Systems*, volume 31, 2018. 13
- [59] Zilong Huang, Xinggang Wang, Jiasi Wang, Wenyu Liu, and Jingdong Wang. Weakly-supervised semantic segmentation network with deep seeded region growing. In *Proceedings of the IEEE Conference on Computer Vision and Pattern Recognition*, pages 7014–7023, 2018. 13
- [60] Jiwoon Ahn, Sunghyun Cho, and Suha Kwak. Weakly supervised learning of instance segmentation with inter-pixel relations. In *Proceedings of the IEEE/CVF Conference on Computer Vision and Pattern Recognition*, pages 2209–2218, 2019. 13
- [61] Peng-Tao Jiang, Qibin Hou, Yang Cao, Ming-Ming Cheng, Yunchao Wei, and Hong-Kai Xiong. Integral object mining via online attention accumulation. In *Proceedings of the IEEE/CVF International Conference on Computer Vision*, pages 2070–2079, 2019. 13
- [62] Yazhou Yao, Tao Chen, Guo-Sen Xie, Chuanyi Zhang, Fumin Shen, Qi Wu, Zhenmin Tang, and Jian Zhang. Non-salient region object mining for weakly supervised semantic segmentation. In *Proceedings of the IEEE/CVF Conference on Computer Vision and Pattern Recognition*, pages 2623–2632, 2021. 13
- [63] Lian Xu, Wanli Ouyang, Mohammed Bennamoun, Farid Boussaid, Ferdous Sohel, and Dan Xu. Leveraging auxiliary tasks with affinity learning for weakly supervised semantic segmentation. In *Proceedings of the IEEE/CVF International Conference on Computer Vision (ICCV)*, pages 6984–6993, October 2021. 13
- [64] Tong Wu, Junshi Huang, Guangyu Gao, Xiaoming Wei, Xiaolin Wei, Xuan Luo, and Chi Harold Liu. Embedded discriminative attention mechanism for weakly supervised semantic segmentation. In *Proceedings of the IEEE/CVF Conference on Computer Vision and Pattern Recognition*, pages 16765–16774, 2021. 13
- [65] Seungho Lee, Minhyun Lee, Jongwuk Lee, and Hyunjung Shim. Railroad is not a train: Saliency as pseudo-pixel supervision for weakly supervised semantic segmentation. In *Proceedings of the IEEE/CVF Conference on Computer Vision and Pattern Recognition*, pages 5495–5505, 2021. 13

Appendix

A. Additional VOC 2012 comparisons

Table 5 compares the results from SEAM [4] with our contributions implemented naively, i.e. not considering the pixel-wise normalization of the CAMs using softmax. We see that a proper normalization is required for the importance sampling to be useful. We also see that the feature similarity loss improves the contour accuracy, although, with a loss of area mIoU. In summary, our contributions work well together and with proper normalization of the CAMs.

In Tab. 7 we show VOC results for state-of-the-art WSSS methods. For completeness, we include those using saliency maps as well, indicated by the “*Sup.*” column. Note however, that the saliency-based methods implicitly use ground-truth segmentation masks since the saliency detectors are trained using pixel-level annotations.

Table 5. Performance on the VOC 2012 *val* set.

Method	Area	Contour
	mIoU	F-score
SEAM	64.5	38.2
SEAM + importance sampling	28.9	20.5
SEAM + feature similarity loss	57.9	40.9
Ours	66.1	47.4

B. Extended ablation study

It might be the case that sampling several pixels could allow for more efficient learning. Therefore, we evaluate our method when varying the number of sampled pixels and averaging the classification loss \mathcal{L}_{cls} accordingly. The results are shown in Tab. 6 where we use $\lambda = 1$. Although CAM results vary slightly we do not observe a significant trend in the performance of the final segmentation predictions.

Table 6. Performance on the VOC *validation* set when varying the number of sampled pixels with $\lambda = 1$. Results computed for CAM pseudo labels (CAM) and DeepLab-v1 predictions (DLB).

#pixels	Area mIoU		Contour F-score	
	CAM	DLB	CAM	DLB
1	55.1	65.8	38.2	46.4
2	55.8	65.9	39.5	46.7
5	56.1	65.8	38.7	46.7
10	56.0	65.6	39.0	45.8
20	56.1	65.7	38.2	45.5
50	55.8	65.4	37.6	45.4
100	56.4	65.9	38.7	45.6

Therefore, we sample only one pixel since it requires the least amount of computations.

In Figs. 5, 6, 7 and 8 we show the performance of the CAM pseudo-labels and the final segmentations, as functions of λ and the feature similarity loss (FSL). These figures are similar to Figs. 2 and 3 of the main paper, but include results also for the CAM pseudo-label performance. Additionally, the plots have a higher resolution of data points in the region of interest, between 0.6 and 1.0 for λ . With max pooling in Figs. 5 and 6, the highest area mIoU occurs at $\lambda = 1$, although the performance at 0.9 is very similar. For the CAM results with GAP, the highest area mIoU occurs at 0.9 in Fig. 7, while the highest mIoU for the final predictions occurs at 0.8 in Fig. 8.

Table 7. Performance on the VOC dataset. The “Sup.” column indicates the supervision used, I for *image-level*, and S for *saliency*.

Method	Backbone	Sup.	<i>val</i>	<i>test</i>	Method	Backbone	Sup.	<i>val</i>	<i>test</i>
CCNN [15]	VGG-16	I	35.3	35.6	SSDD [42]	ResNet-38	I	64.9	65.5
EM-Adapt [11]	VGG-16	I	38.2	39.6	SEAM [4]	ResNet-38	I	64.5	65.7
STC [17]	VGG-16	I+S	49.8	51.2	OAA [61]	ResNet-101	I+S	65.2	66.4
SEC [16]	VGG-16	I	50.7	51.7	CONTA [43]	ResNet-38	I	66.1	66.7
AugFeed [39]	VGG-16	I	54.3	55.5	CDA [44]	ResNet-38	I	66.1	66.8
AE-PSL [54]	VGG-16	I+S	55.0	55.7	MCIS [45]	ResNet-101	I	66.2	66.9
MDC [55]	VGG-16	I+S	60.4	60.8	LIID [23]	ResNet-101	I+S	66.5	67.5
MCOF [56]	ResNet-101	I+S	60.3	61.2	ECS-Net [46]	ResNet-38	I	66.6	67.6
DCSP [57]	ResNet-101	I+S	60.8	61.9	ICD [40]	ResNet-101	I+S	67.8	68.0
SeeNet [58]	ResNet-101	I+S	63.1	62.8	CGNet [47]	ResNet-38	I	68.4	68.2
DSRG [59]	ResNet-101	I+S	61.4	63.2	CPN [48]	ResNet-38	I	67.8	68.5
AffinityNet [6]	ResNet-38	I	61.7	63.7	NSROM [62]	ResNet-101	I+S	68.3	68.5
ICD [40]	ResNet-101	I	64.1	64.3	AuxSegNet [63]	ResNet-38	I+S	69.0	68.6
IRNet [60]	ResNet-50	I	63.5	64.8	PMM [38]	ResNet-38	I	68.5	69.0
CIAN [41]	ResNet-101	I	64.3	65.3	EDAM [64]	ResNet-101	I+S	70.9	70.6
FickleNet [7]	ResNet-101	I+S	64.9	65.3	EPS [65]	ResNet-101	I+S	71.0	71.8
					Ours	ResNet-38	I	66.1	66.6

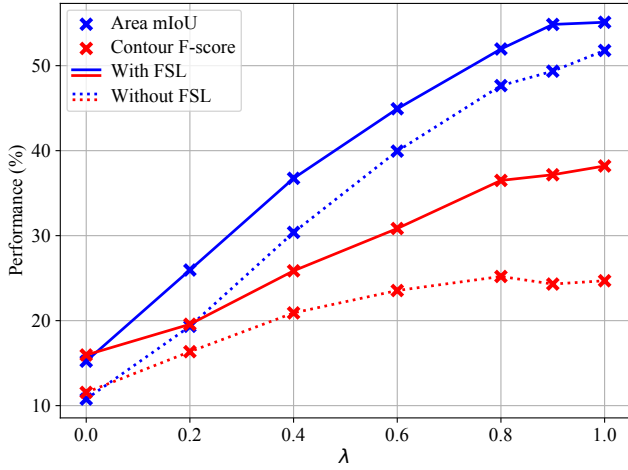


Figure 5. CAM performance with global max pooling.

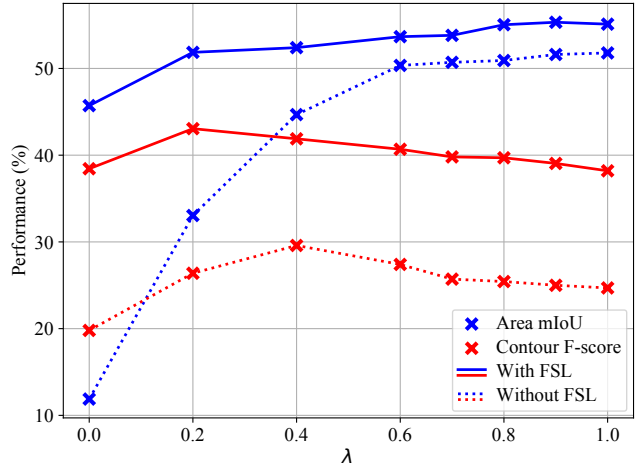


Figure 7. CAM performance with global average pooling.

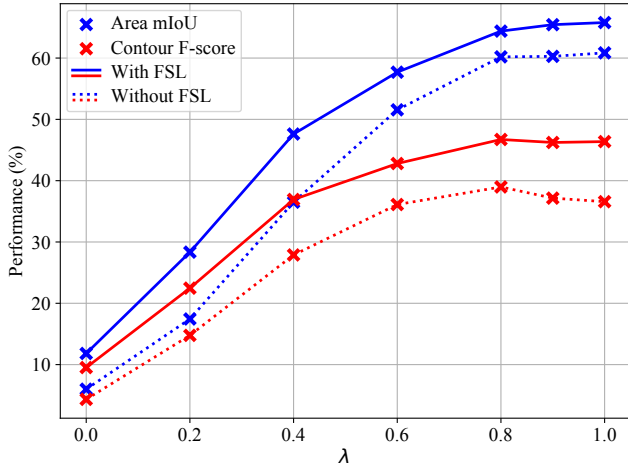


Figure 6. Final performance with global max pooling.

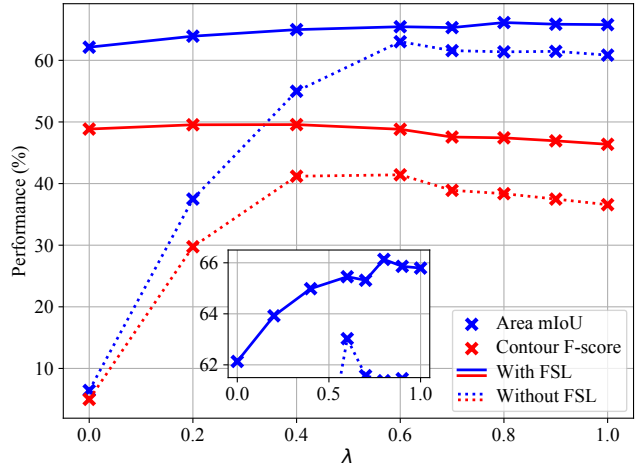


Figure 8. Final performance with global average pooling.